Special Issue 19th KKMGiIG **Open Access**

Marcin Bujko, Marta Bocheńska*, Piotr Srokosz, Ireneusz Dyka

Modernized Resonant Column and Torsional Shearing Apparatus With Multipoint Contactless Displacement Detection System

https://doi.org/10.2478/sgem-2023-0018
received February 26, 2023; accepted September 11, 2023.

Abstract: In this study, a modification of resonant column/torsional shearing (RC/TS) apparatus was proposed to perform a qualitative analysis of a noncohesive soil specimen vibration during RC tests. An additional multipoint displacement detection system was installed in the RC/TS WF8500 device. In the new measuring system, 48 mini-magnets are attached to the side surface of a cylindrical soil specimen, creating a regular grid of measuring points. Around 48 Hall sensors (Honeywell SS495A1) are used to measure changes in the magnetic field strength due to the movement of the corresponding magnets on the surface of the specimen subjected to dynamic torque. The Hall sensor generates an analog signal that is proportional to the change in the magnetic field. The measurements are collected with a newly developed data acquisition system that consists of a set of analog-to-digital converters and a set of ARM (Advanced RISC (Reduced Instruction Sets Computing) Machine) microcontrollers. The measurement system is controlled with a dedicated software, *ControlRec*, developed by the authors. The measurements are taken synchronically with and independently from the standard RC test procedure. The new measuring technique allows to observe displacements of the 48 points on the specimens' surface with over 4 times higher sampling rate than in the original measuring system. As a result, additional effects related to the mechanical wave propagation through soil specimen were observed (local disturbances in distribution of vibration amplitudes or significant displacements near the bottom end of the specimen, which is assumed to be fixed in the standard RC/TS results analysis), that could not be identified using the standard equipment of the device.

Keywords: resonant column; noncohesive soil; Hall effect sensors; dynamic effects.

1 Introduction

A development of accurate and detailed description of soil reaction to dynamic loading requires the use of high-precision laboratory measuring equipment. Although currently available technologies create vast opportunities for extending observations and measurements, most of the laboratory devices (Li et al., 2013) for soil dynamic properties determination are designed for taking measurements only of some resultant value at one point of a tested specimen. To simplify the interpretation of test results radical assumptions are made about the distribution of a measured behavioral aspect throughout the specimen. For example, in the torsional shearing (TS) test specimen, deformation is measured at one point near the upper end of the specimen, where the torque is applied. The distribution of torsional deformation along the specimen's height is assumed to be linear. The measured resultant values (displacements) represent the state of the material throughout the whole specimen and are used in calculations of mechanical parameters (e.g., stiffness parameters). The testing procedure is automated, and the approach is convenient to use in practice. However, it provides little or no information about the material's behavior inside or at other points on the surface of the specimen. It is a known fact (Wichtmann & Triantafyllidis, 2020) that measuring of deformation at one point of a material does not specify the deformation distribution throughout the whole volume of the material. For the purpose of results' interpretation, certain assumptions need to be adopted.

***Corresponding author: Marta Bocheńska,** University of Warmia and Mazury in Olsztyn, Olsztyn, Poland, E-mail: marta.bochenska@uwm.edu.pl
Marcin Bujko, Piotr Srokosz, Ireneusz Dyka, University of Warmia and Mazury in Olsztyn, Olsztyn, Poland

Displacements can be measured on the surface of a soil specimen using contact or contactless measurement techniques, like LVDT (Linear Variable Differential Transformer) sensors (Huawen, et al., 2019), fiberoptic sensors (Xu, 2017), optical methods (Iskander, 2010) including photogrammetry and particle image velocimetry (PIV) (White, et al., 2003), (Gill & Lehane, 2001), chemiluminescent sensors (Kuang, 2018), or optical flow (Srokosz, et al., 2021). And inside a specimen, using X-ray tomography or magnetic resonance imaging (Desrues, et al., 2006), (Tyrologou, et al., 2005), (Kong, et al., 2018) which is often too expensive, economically unjustified and available only for the best-equipped geotechnical laboratories.

The resonant column (RC) along with the TS tests are currently considered most accurate for laboratory determination of shear modulus G and damping ration D in small–medium strain range (Drnevich, et al., 2015), (Darendeli, 2001). The RC soil testing is also relatively simple in terms of measurement interpretation and easy to operate (Massarsch, 2004), (Mayne, et al., 2009). A commonly used model for RC result analysis is a rigid rod subjected to torsional vibration that has a specific number of degrees of freedom depending on the support conditions. Different modes of vibration or possible support imperfections are not considered. It was previously discovered (Srokosz, et al., 2021) that the theoretical assumptions about the strain distribution inside the specimen subjected to torque in RC/TS apparatus should be considered overly simplified in some cases. The loading transfer from the drive system to the material and the force distribution in the specimen can depend on a variety of technical issues. For example, a slip effect can occur both on the *top cap-specimen* and *porous stone-specimen* surface use of optical (Bujko, et al., 2017), (Bujko, 2021). In (Srokosz, et al., 2021) measurements allowed to observe that during cyclic slow-changing loading not the whole of the specimen volume was experiencing displacements (contrary to the original assumption). This observation could not be made without introducing an external measuring technique, as the standard device allows only for one-point displacement measurements (near the top cap). The assumption deviation should perhaps be considered also during the dynamic tests. Another important issue in the original construction of the device is that the proximity sensors (measuring the horizontal displacements) are attached to the drive system and therefore do not measure the displacements directly on the specimen's surface. This, along with the aforementioned slip effect, can surely contribute to the measurement uncertainty.

Unlike many laboratory devices, the RC/TS apparatus (model WF8500, used in this study) has a design that allows for introducing modifications (Anestis & Surendra, 1990), (Bae & Bay, 2009). The internal, polycarbonate cylinder has numerous sockets, grommets, and a lot of free space that allow for the installation of additional components without radical modifications. In Srokosz, et al., (2021), the authors installed 5 accelerometers to the specimen's surface in order to observe and analyze specimen vibration on several levels along the specimen's height. The accelerometers attached to the specimen's surface detected some additional dynamic effects, which were not visible in standard test results. The shape of the disturbances resembled a standing wave effect, so it might be suggested that wave reflection and interference can affect the final result. Especially if the waves would interfere near the resonant frequency value. However, many wave propagation and interaction phenomena can contribute to the observed anomalies.

To continue the investigation of local vibration disturbances in the specimen, in this study the authors proposed a new multipoint measurement system. In the proposed modification of the standard device, 48 small neodymium magnets are attached to the lateral surface of the specimen. The magnets' placement creates a regular grid of measuring points: 48 Hall sensors fixed to the internal cylinder and their location corresponds with the arrangement of the magnets. Hall sensors react to the changes in magnetic field caused by the movement of the magnets and produce an analog signal proportional to those changes. The measurement is contactless, so the influence on the specimen deformation is minimized. The obtained results allowed to conduct a qualitative analysis of the specimen vibration on the whole side surface. Some local vibration disturbances were observed that are not compliant with the theoretic model for RC test results interpretation and that could not be detected with the standard device's equipment.

2 Materials and methods

2.1 Soil specimens

Noncohesive soil specimens were used for the experiments in this study. The choice of the tested material (silica sand) was based on Wichtmann's habilitation thesis (Wichtmann, 2016), who used this type of soil to perform tests in RC. Wichtmann performed about 650 RC tests with additional measurement of the pressure wave propagation

Table 1: The physical parameters of soil.

Soil type	G [-]	$_0$ [mm]	$_0$ [mm]	$_0$ [mm]	[-]	[-]	$_n$ [-]	[g/cm³]
silica sand	2.65	0.33	0.41	0.14	3.0	0.68	0.41	1.86

Gs—specific gravity (Wichtmann & Triantafyllidis, 2020), dS0, d60, d10—values of the particle diameter at 50, 60, and 10% in the cumulative distribution, U—uniformity coefficient, max—maximum void ratio, min—minimum void ratio, ρ—bulk density

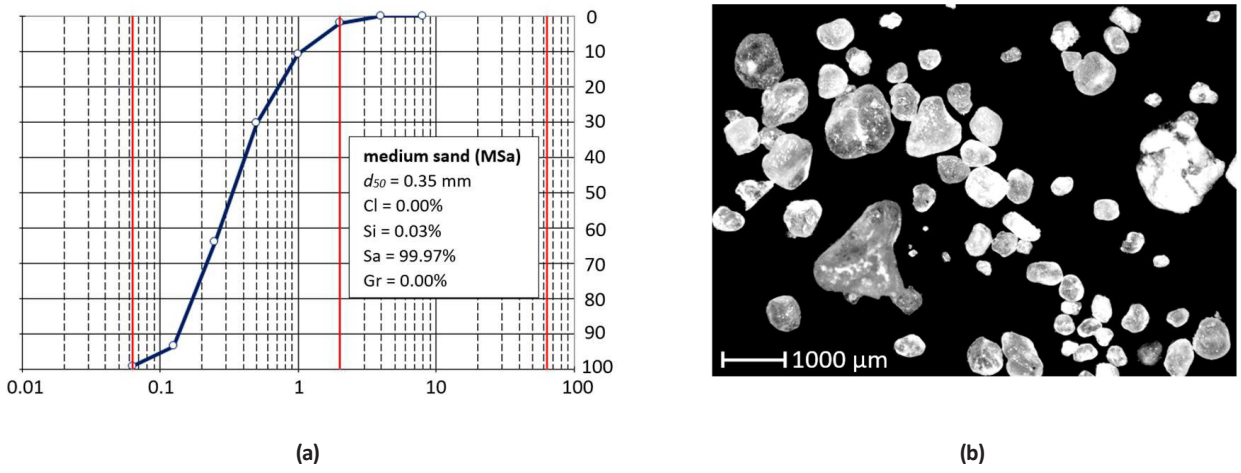

Figure 1: Tested material **(a)** grain size distribution **(b)** microscopic image of tested sand's grains (Dyka, et al., 2017).

velocity (P-wave) on noncohesive soil specimens with 65 different grain size curves. One of them has been reproduced for the purposes of this work.

The sand is classified as a poorly graded sand with a uniformity coefficient CU value of 3.0 (see **Table 1** and **Figure 1**). Geometrical and physical parameters of tested soil are presented in **Table 1**.

The maximum dry density and the optimum moisture content of the sand were determined through the Standard Proctor Compaction Test. The specimens were prepared with the optimum moisture content (3.0–3.5%).

2.2 RC/TS apparatus

The modifications proposed in this study were introduced to the device made by Wykeham Farrance (model WF8500). It is a conventional fixed-base free top version of the apparatus (ASTM Standard, 2000). The WF8500 is an RC device with TS and free decay (FD) operation modes. The device is designed to measure soil stiffness parameters (shear modulus G and damping ratio D). A cylindrical soil specimen or sample is installed in the device (placed between a porous stone and a top cap and covered with elastic membrane). The torque T is applied through the cyclic or dynamic motion of the top cap. In RC mode, the top cap vibrates with gradually increasing frequency f and the specimen reaction (twist angle) to the excitation is measured and analyzed. The initial value of shear modulus G_0 can be then obtained using the following formula that takes into account the elastic waves propagation:

$$G_0 = G = \rho V_s^2 = \rho \frac{4\pi^2 f_r^2 L^2}{\beta^2} \tag{1}$$

where: ρ—bulk density of the material (soil); Vs —shear wave velocity, fr—resonant frequency; L—height of the specimen; β—angle that can be derived from:

$$\frac{I}{I_0} = \beta \cdot \tan(\beta) \tag{2}$$

I – mass moment of inertia of the specimen; I_0 – mass moment of inertia of the drive system.

The mass moment of inertia of the drive system can be calculated using geometry and special distribution of all the elements, but the procedure would be challenging and most likely affected by errors (Clayton et al., 2009). Therefore I_0 is usually obtained during a calibration process (using metal rods of a known torsional rigidity) (Bui et al., 2019).

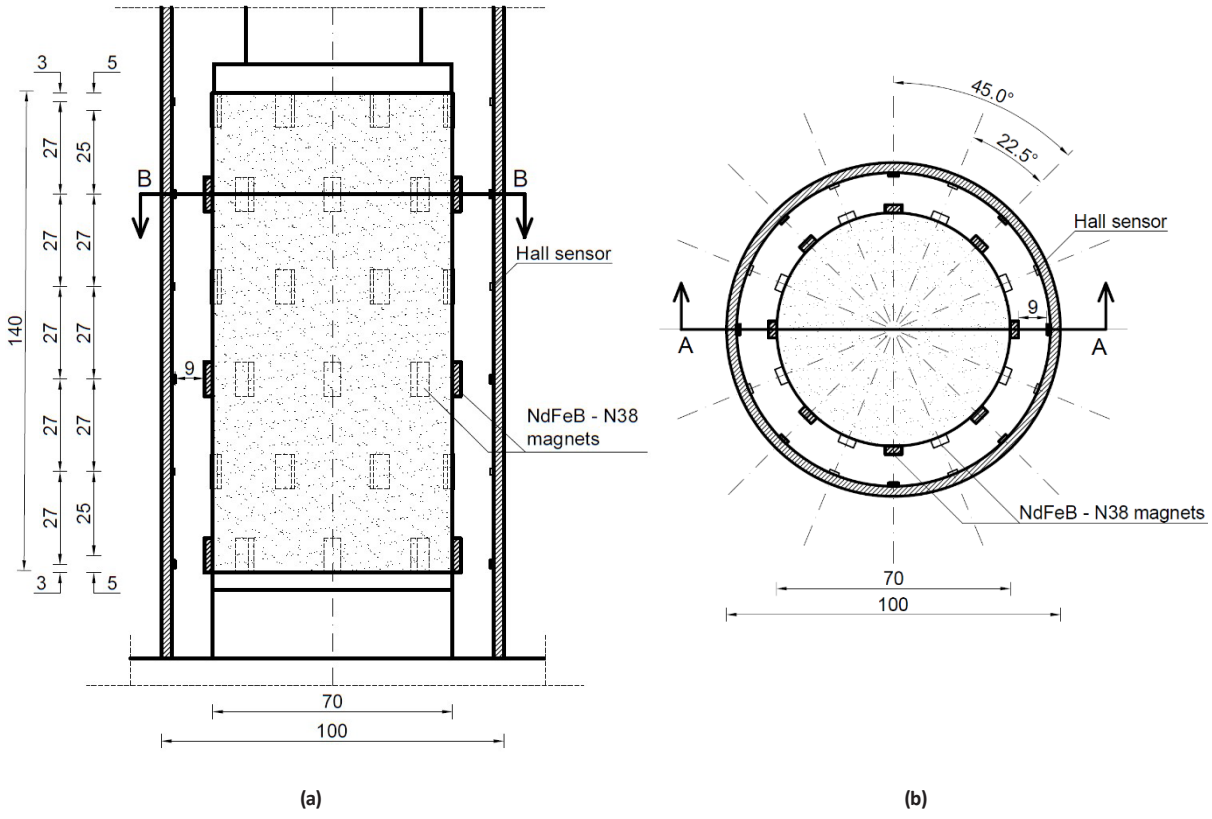

Figure 2: The arrangement of magnets on the specimen's surface and Hall sensors on the internal cylinder **(a)** vertical (A-A) section; the middle dimension line refers to the placement of the Hall sensors and the right dimension line refers to the magnets, **(b)** horizontal (B- B) section [mm].

The device works in a frequency spectrum of 10–300 Hz. The resonant frequency fr can be determined through gradually increasing (incrementally or smoothly) the torsional vibration frequency. Resulting time–angle relationship can be transformed into a frequency–angle graph. The resonant frequency corresponds to the maximum twist angle (the peak on the graph). A detailed description of the preparation, test, and standard results interpretation can be found e.g. in (Dyka & Srokosz, 2012) and (Dyka & Srokosz, 2014).

2.3 Modified RC/TS apparatus

In this study, a contactless displacement detection method is proposed. In the proposed modification, 48 small neodymium magnets NdFeB–N38 (10 x 5 x 2.5 mm, 1 g) are attached to the specimen's surface using adhesive tape. The placement of the magnets corresponds with the arrangement of 48 Hall sensors (Honeywell SS495A1), which are glued to the internal cylinder. The exact placement of the magnets and the sensors is presented in **Figure 2**. As the specimen undergoes torsional deformation, the magnets change their position. The Hall sensors detect changes in magnetic field strength due to the movement of magnets. The Hall sensor produces analog signal that is proportional to the change in magnetic field. The resulting changes in voltage can be translated into changes in displacement. The data is collected and converted to digital output by a data acquisition system developed by the authors specifically for these tests. An operational amplifier connected to an analog-to-digital converter sends data to a dedicated software through an AVR microcontroller. The measurements can be taken during the RC or TS test and the data from the Hall sensors is collected independently from the standard RC/TS software.

The additional components added to the standard RC/TS equipment are as follows:

1. A polycarbonate cylinder with a regular grid of Hall sensors (**Figure 3**),
2. A communications interface (**Figure 4**),

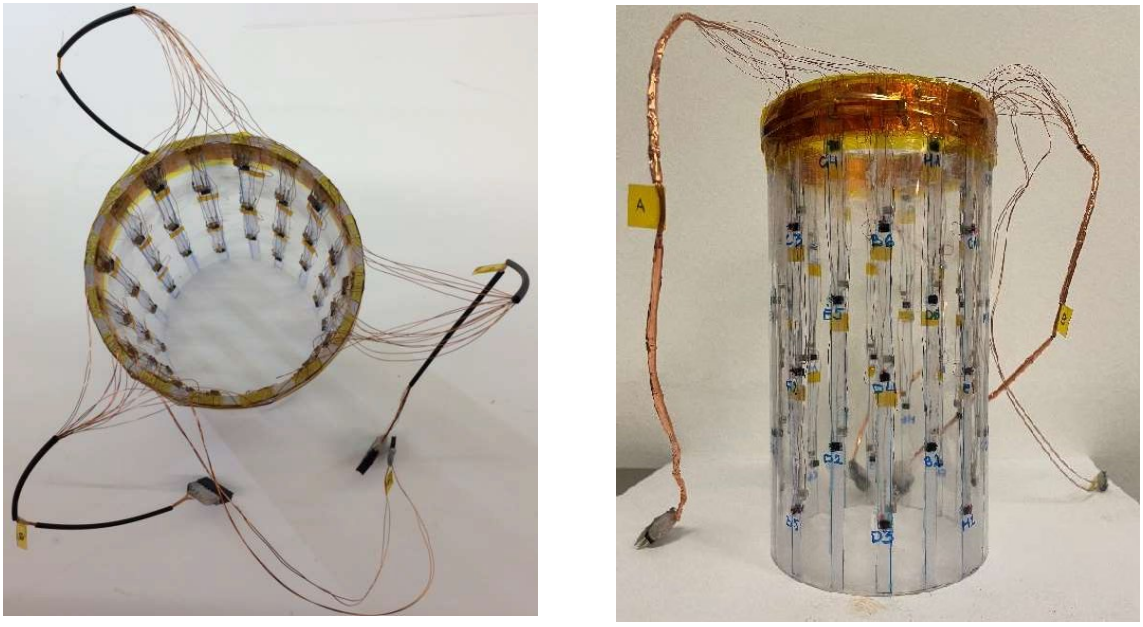

(a) (b)

Figure 3: Polycarbonate cylinder with Hall sensors installed on the surface **(a)** top view, **(b)** side view.

Figure 4: The inside view of the communications interface.

a. A signal conditioning system (low-noise voltage stabilizers, resistor voltage dividers with high temperature stability and ultralow tolerance),
b. 24-bit analog-to-digital converters (Microchip MCP3903),
c. A control module (a set of microcontrollers Raspberry Pi PICO RP-2040 with dual-core processors ARM Cortex M0+ operating at a frequency of 120 MHz),

3. A dedicated software *ControlRec* (**Figure 5** shows the User Interface) for the measurement system control. The software allows for data collection and automatic interpretation with 16-bit resolution and 4 or 8 Hz sampling rate. Higher sampling rate (comparing to the standard RC/TS device's equipment) allows for much more detailed observation of displacements on the surface of the specimen vibrating with the resonant frequency.

2.4 Specimen preparation and testing procedure

In the RC/TS apparatus cylindrical soil specimens are tested. All specimens have the following dimensions: L = 140 *mm* (height) and d = 70 *mm* (diameter). The weight and the exact geometrical dimensions of the specimens are measured during the experiment. The specimen

Figure 5: User Interface of the measurement system control software.

preparation and the testing procedure consist of the following steps:

1. A soil specimen is shaped in a latex membrane and a rigid cylindrical form. The material is compacted with a hand rammer (about 25 strokes per layer) in 5 layers.
2. After the specimen is installed, the rigid form is disassembled and the RC/TS device chamber equipment is assembled (internal cylinder, drive system, measurement system, and external cylinder).
3. The soil specimen is subjected to isotropic pressure of 50 kPa for 24 hours before performing an RC test.
4. A series of preliminary RC tests is performed for torque amplitudes not exceeding 5% of the maximum torque amplitude that can be applied in RC/TS apparatus (0.01 V, 0.02 V, 0.05 V, 0.1 V, 0.2 V, and 0.5 V). The series of tests is carried out to determine the minimum and maximum value of frequency that should be applied during the tests. The resonant frequency is expected to be found in that specified range.
5. The specimen is unloaded and the device equipment is disassembled.
6. The magnets are attached to the membrane surface with adhesive tape. The specimen with the attached magnets is presented in **Figure 6.** The magnets are placed in the following pattern: the north pole and south pole are facing outward alternately (for the laterally neighboring magnets). The magnets are arranged this way not to reduce the sensor's signal when a neighboring magnet is moving toward the sensor.
7. The specimen is covered with the additional internal cylinder with Hall sensors installed on its internal surface. The RC/TS device chamber equipment is assembled.
8. The soil specimen is subjected to isotropic pressure of 50 kPa for 24 hours.
9. A series of RC tests (see point 4.) is performed to assess the influence of the magnets' installation on the resonant frequency of the *magnets-specimen-device* system.
10. The main series of RC tests is performed for torque amplitudes in the full range (1 V–10 V in 1 V increments).
11. Additionally, after the main series of experiments, TS tests are performed.

After conducting the RC tests (the main experiment), TS tests were conducted with a very low frequency. As the full calibration was not performed in this study, the cyclic, slow-changing tests were necessary to assess how small deviations in the magnet–sensor distance affect the Hall sensor measurements. This information could not be obtained during the RC tests, as additional dynamic effects could be expected to occur in the material.

The TS tests were performed with the loading path parameters presented in **Table 3**.

Figure 6: The sand specimen covered with a latex membrane and magnets attached to the surface The main RC tests were carried out with the input parameters presented in **Table 2**.

Table 2: The RC test input parameters.

Testing mode	Test number	p [kPa]	f_0 [Hz]	f_f [Hz]	A [V]
Resonant column	1.	50	100	200	1.0
	2.		80	180	2.0
	3.		60	160	3.0
	4.		60	160	4.0
	5.		50	150	5.0
	6.		50	150	6.0
	7.		50	150	7.0
	8.		40	140	8.0

p—confining pressure, f_0—initial frequency (min. value of the frequency spectrum), ff—final frequency (max. value of the frequency spectrum), A—amplitude of torque

Table 3: The TS test input parameters.

Testing mode	p [kPa]	f [Hz]	A [V]	n [-]
Torsional shearing	50	0.02	5.0	3

p—confining pressure, f—frequency of torque change, A—amplitude of torque, n—number of loading cycles

Table 4: RC test results.

RC test number	f_r [Hz]	γ [%]	G [MPa]
1.	145.45	0.0069	84.51
2.	125.61	0.0116	62.88
3.	115.48	0.0144	53.27
4.	107.60	0.0185	46.18
5.	101.01	0.0242	40.69
6.	96.01	0.0312	36.73
7.	88.81	0.0388	31.45
8.	83.19	0.0491	27.60

fr—resonant frequency, γ—strain, G—shear modulus

3 Results and discussion

The RC test results obtained with the original measuring system are presented in **Table 4.**

Figure 7 shows the results of the RC test (angle–frequency graph) and the fast Fourier transform (FFT) analysis for different torque amplitudes (0.02 V, 0.1 V, and 0.2 V). The results are compliant with the well-known and documented phenomenon that the resonant frequency value (and therefore the shear modulus G) depends on the shear strain level. The higher is the strain level (here, the amplitude), the lower is the stiffness of the material (G). For the considered amplitude range (0.02 V–0.2 V) the calculated G values decreased from 72 MPa to 63 MPa (13%).

The results also confirm that repeating the experiment affects the resonant frequency in a non-negligible way. **Figure 8** shows the observed stiffness degradation between the subsequent loading cycles (for the amplitude 0.2 V). Three full loading cycles were performed for two amplitude values (0.1 V and 0.2 V). The obtained G values decreased from 67 MPa to 65 MPa (3%) and from 60 MPa to 57 MPa (5%), respectively.

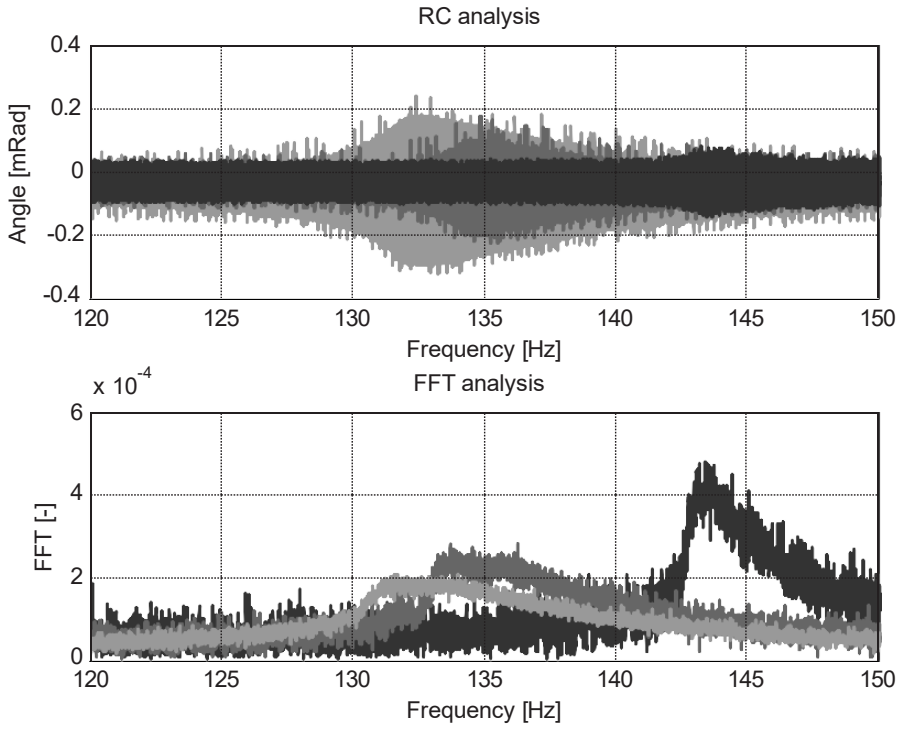

Figure 7: Influence of the torque amplitude on the resonant frequency of the specimen (light gray—0.02 V, medium gray—0.1 V, black—0.2 V).

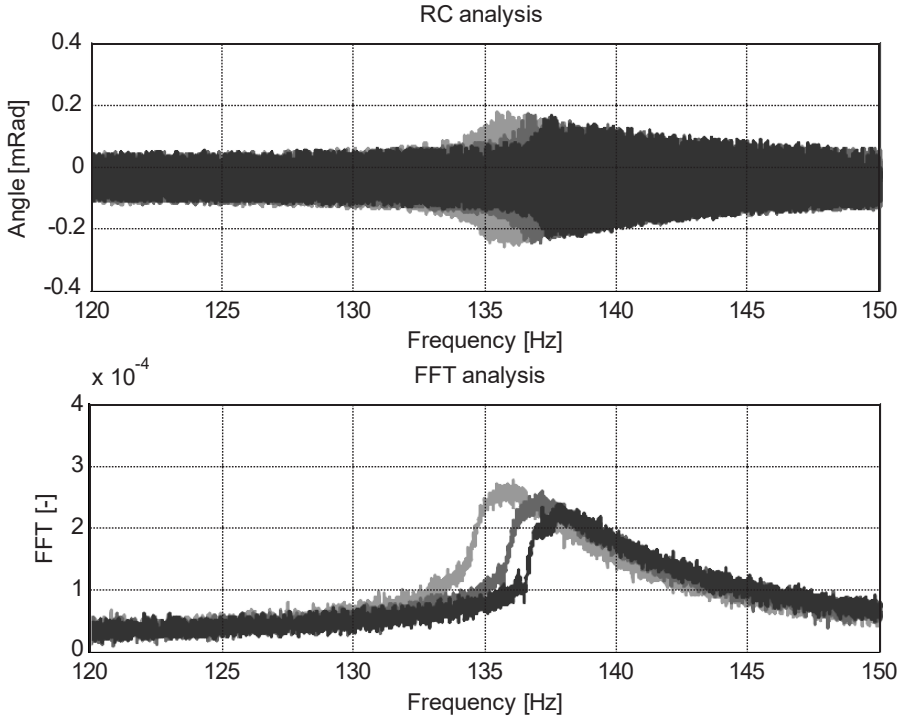

Figure 8: Influence of the subsequent loading cycles (test repetitions) on the resonant frequency value. The torque amplitude value is 0.2 V; black—first cycle; medium gray—second cycle; light gray—third cycle.

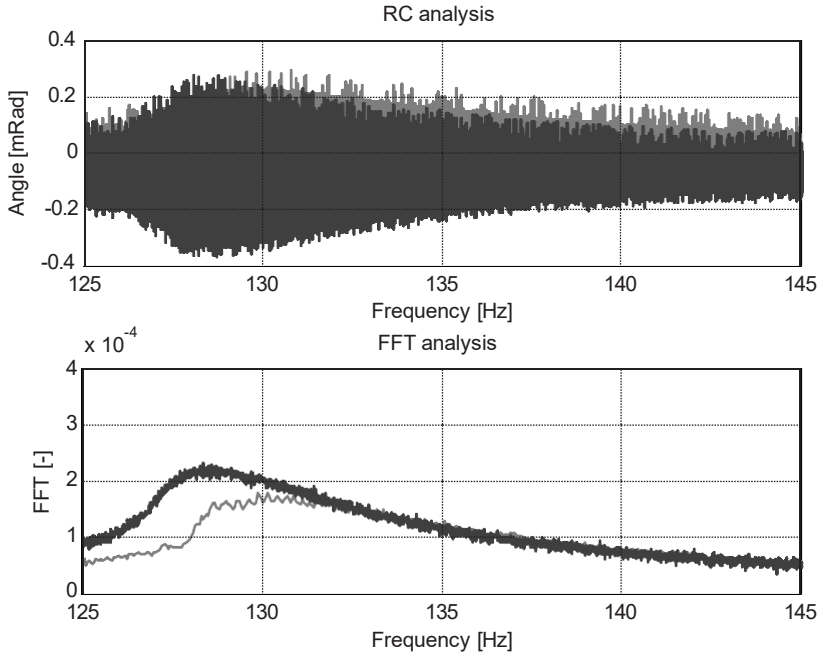

Figure 9: Influence of the magnets' installation on the resonant frequency. The torque amplitude is 0.2 V; black—the specimen without magnets; gray—the specimen with the magnets attached to the surface.

There is a distinct relationship between the specimen's mass (and the mass moment of inertia) and the resonant frequency. The magnets attached to the specimen's surface increase the resonant frequency of the *specimen-magnets-device* system. For the torque amplitude 0.2 V the G value increased from 58 MPa to 67 MPa (16%). It can be argued that the influence of the installed magnets partially compensated the decrease in G value caused by the previous loading cycles.

In **Figure 9,** the results for the specimen with and without magnets are compared.

Along with the series of RC tests, a TS test was conducted. A nondynamic test was necessary to assess the quality of magnet–sensor interaction. Considering the facts that

1. there is a nonlinear relationship between the magnet–sensor distance and the sensor's response,
2. exceeding a critical value of magnet–sensor distance (which depends on the magnet's geometry and material) results in a complete loss of signal from the sensor, only the qualitative result analysis was performed.

The displacements of the 48 points on the lateral surface of the specimen detected by the Hall sensors during the TS test are presented in **Figure 10**.

The conducted TS test constitutes a point of reference for a proper analysis of the RC tests results. It is necessary to observe the Hall sensors' reaction to the relatively slow movement of magnets to consider the differences in horizontal sensor–magnet distances and apply this to RC results' analysis. It should be stressed that it has provided information about the measuring system and not about the material.

The TS test was also necessary for the following:

1. A phase shift correction. The phase shift in signals coming from neighboring sensors is related to the opposite orientation of the neighboring magnets' poles.
2. Estimation of the distance between each Hall sensor and the corresponding magnet. The results of the RC tests (**Figure 11**) were adjusted for the relative differences in magnet–sensor positions.

About 77% of the Hall sensors detected changes in the position of magnets The results obtained with those sensors were used for further analysis of the RC tests.

During the performed RC tests, most of the sensors detected the expected specimen reaction to the applied dynamic loading of changing frequency. The signal characteristics are similar to the standard RC proximity sensors readings, that is, there is a distinct maximum

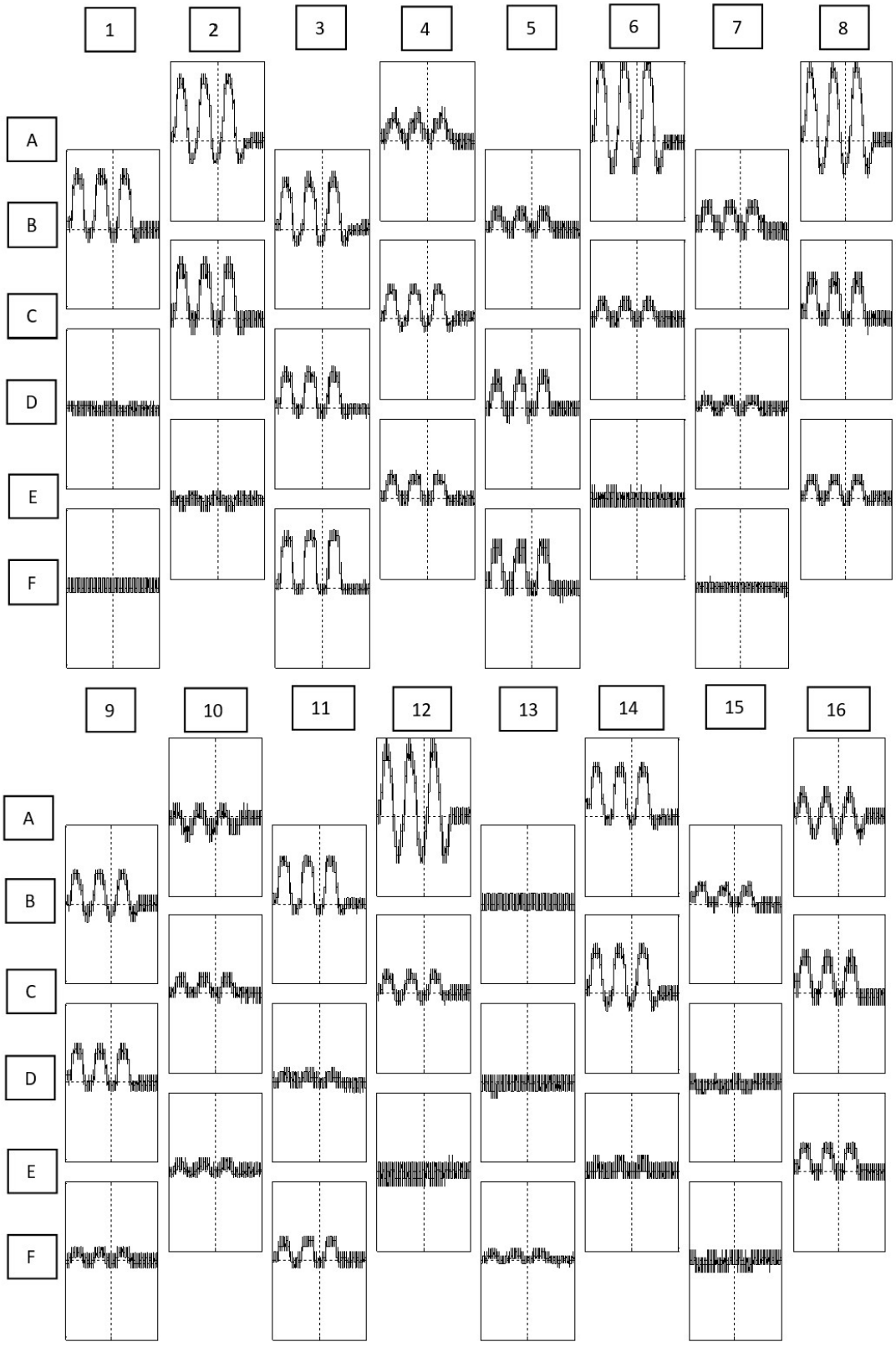

Figure 10: Results of the TS test for amplitude of 5 V. Raw data from the Hall sensors during the TS test. The arrangement of the graphs corresponds with the location of the sensors.

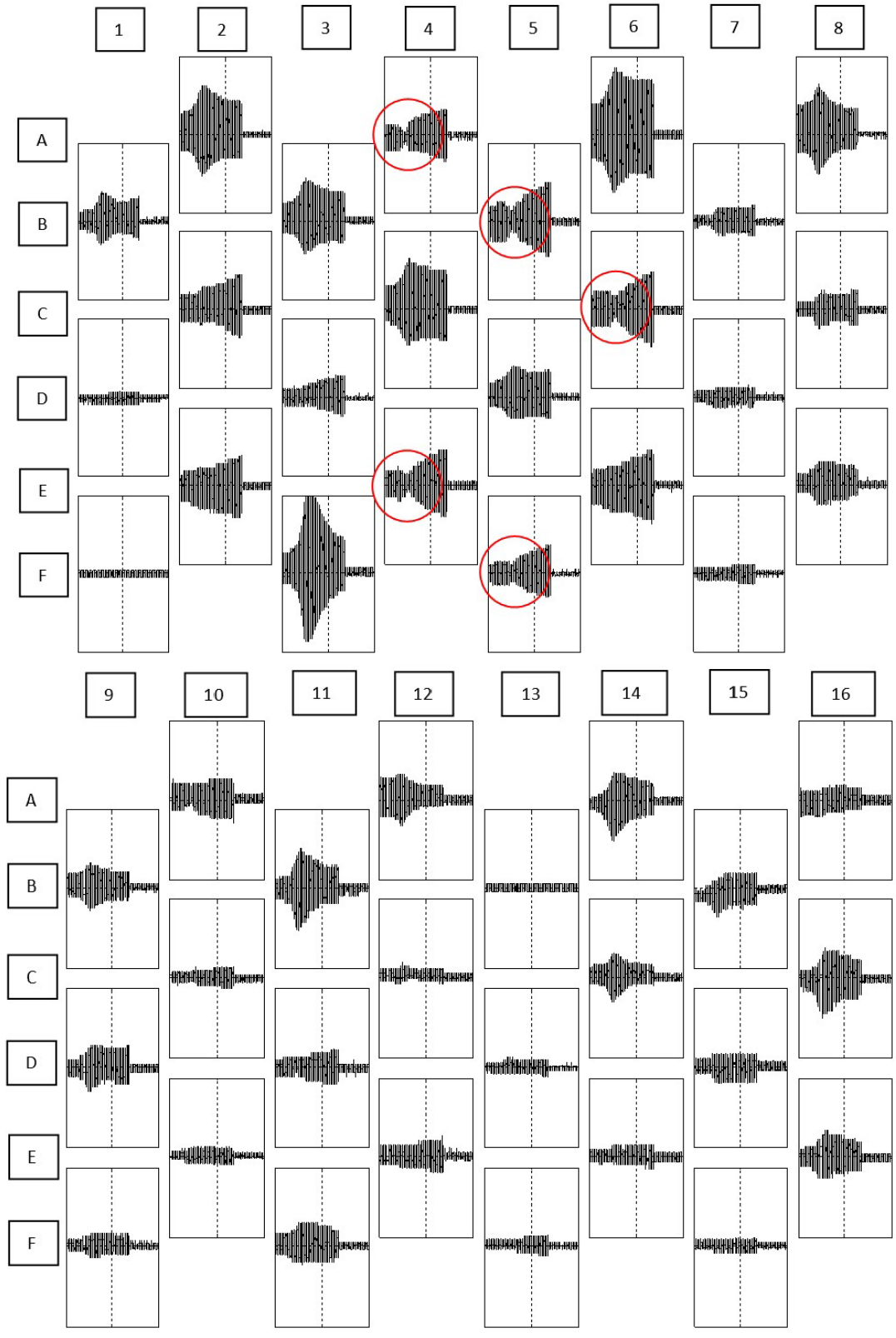

Figure 11: Results of one of the RC tests for the amplitude of 8 V. Raw data from the Hall sensors. The arrangement of the graphs corresponds with the location of the sensors.

amplitude value corresponding with the resonant frequency value.

Careful analysis of the obtained data series shows that:

1. In several measuring points during the forced vibration a local minimum in amplitude value is detected at the time when the resonance is expected to occur (see the series A4, B5, C6, E4 and F5 marked with circles in **Figure 11**).
2. The distribution of amplitudes along some of the vertical lines is significantly disturbed (disproportionately to the observed differences in reaction to TS loading). For example, in column no. 16 (**Figure 11**) there is a noticeably higher amplitude detected near the middle of the specimen's height (C16). This is not compliant with the TS test results, which suggests that the amplitudes for A16 and C16 should be similar (see **Figure 10**). This effect is also observed in column no. 3. The amplitude for location F3 is much higher than for B3 (which is also not confirmed during the TS test).
3. The fixed bottom assumption is not met. The detected changes in magnetic field strongly suggest that magnets placed near the bottom end of the specimen (see locations F3, F5 or F11) experience significant displacements.

4 Conclusions

The proposed multipoint displacement detection method allowed to observe some of the complex effects and disturbances related to mechanical wave propagation through a noncohesive soil specimen. The following main conclusions can be drawn from this study.

1. During the forced vibration (RC test), the vibration amplitudes distribute disproportionately along the specimen's height. In some regions (measuring points) on the specimen's surface there is an observable dampening of the amplitude at the time when the resonant frequency is detected with standard RC equipment and other Hall sensors. The effects should be studied further, and additional experiments are needed to assess the influence of other factors on the obtained results.
2. The performed experiments confirmed that the bottom end of the specimen cannot be considered as fixed. The points near the bottom end undergo significant displacements both during the TS and RC tests. As a consequence, the averaged strain obtained with the standard RC/TS WF8500 measuring equipment (proximity sensors, accelerometers) is affected by a non-negligible error.
3. It should be stressed that this article presents the results of a qualitative research. The performed experiments should be treated as a preliminary research that allowed to identify the aforementioned issues. In order to take accurate measurements of the displacements, a precise calibration of the measuring system is required.

The authors aim to develop the proposed modification of the RC/TS apparatus in future research to ensure accurate measurements of displacements that can be used for further interpretation of soil dynamic properties.

Acknowledgment: The first author acknowledges that this work is a result of his internship at the Universitat Politècnica de Catalunya—BarcelonaTECH Department de Matemàtiques EPSEB, UPC, (Spain) cofinanced by the European Union under the European Social Fund (Operational Program Knowledge Education Development), implemented in the project Development Program of the University of Warmia and Mazury in Olsztyn (POWR.03.05.00-00-Z310/17).

References

[1] Anestis, S., & Surendra, K. (1990). The modified "stiffened" Drnevich resonant column apparatus. *Soils and Foundations, 30*(3), pp. 53-68.

[2] ASTM Standard. (2000). *Standard Test Methods for Modulus and Damping of Soils by the Resonant-Column Method (ASTM D4015- 92(2000))*. doi:10.1520/D4015-92R00

[3] Bae, Y.-S., & Bay, J. (2009). Modifications of resonant column and torsional shear device for the large strain. *Computers and Geotechnics, 36*(6), pp. 944-952. doi:10.1016/j.compgeo.2009.02.004

[4] Bui, M. T., Priest, J. A., & Clayton, C. (2019). A New Calibration Technique to Improve Data Reduction for Stokoe Resonant Column Test: Energy and Geotechnics. *Proceedings of the 1st Vietnam Symposium on Advances in Offshore Engineering*, (pp. 43-48). doi:10.1007/978-981-13-2306-5_3

[5] Bujko, M. (2021). *Identification and description of elasto-plastic deformation of soil in the range of small strain. [Doctoral dissertation, Bialystok University of Technology].*

[6] Bujko, M., Srokosz, P. E., & Dyka, I. (2017). Use of Optical Method for Improvement of Soil Dynamic Tests in Torsional Shear Apparatus.

[7] *2017 Baltic Geodetic Congress (BGC Geomatics)* (pp. 404-408). Gdansk: IEEE. doi:10.1109/BGC.Geomatics.2017.45

[8] Clayton, C. R., Priest, J. A., Bui, M. T., Zervos, A., & Kim, S. G. (2009). The Stokoe resonant column apparatus: effects of

stiffness, mass and specimen fixity. *Géotechnique, 59*(5), pp. 429-437. doi:10.1680/geot.2007.00096

[9] Darendeli, M. B. (2001). *Development of a new family of normalized modulus reduction and material damping curves [Doctoral dissertation, The University of Texas at Austin]*. ProQuest Dissertations Publishing.

[10] Desrues, J., Viggiani, G., & Bésuelle, P. (Eds.). (2006). *Advances in X-ray tomography for geomaterials*. ISTE.

[11] Drnevich, V., Werden, S., Ashlock, J., & Hall, J. (2015). Applications of the New Approach to Resonant Column Testing. *Geotechnical Testing Journal, 38*, p. 20140222. doi:10.1520/GTJ20140222

[12] Dyka, I., & Srokosz, P. E. (2012). Badania gruntu w aparacie skrętnego ścinania RC/TS. Część 1. *Inżynieria Morska i Geotechnika, 6*, pp. 700- 707.

[13] Dyka, I., & Srokosz, P. E. (2014). Badania gruntu w aparacie skrętnego ścinania RC/TS. Część 2. *Inżynieria Morska i Geotechnika, 2*, pp. 118- 129.

[14] Dyka, I., Srokosz, P. E., & Bujko, M. (2017). Influence of grain size distribution on dynamic shear modulus of sands. *Open Engineering, 7*, pp. 317–329.

[15] Gill, D., & Lehane, B. (2001). An optical technique for investigation soil displacement patterns. *Geotechnical Testing Journal, 24*(3), pp. 324- 329.

[16] Huawen, X., Fook, H. L., Kai, Y., Jiahui, H., & Yong, L. (2019). Miniature LVDT setup for local strain measurement on cement-treated clay specimens. *Marine Georesources & Geotechnology, 37*(5), pp. 568-577. doi:10.1080/10641 19X.2018.1460428

[17] Iskander, M. (2010). Optical Techniques in Geotechnical Engineering. In *Modelling with Transparent Soils. Springer Series in Geomechanics and Geoengineering*. (pp. 5-18). Springer. doi:10.1007/978-3-642-02501-3_2

[18] Kong, L., Sayem, H. M., & Tian, H. (2018). Influence of drying–wetting cycles on soil-water characteristic curve of undisturbed granite residual soils and microstructure mechanism by nuclear magnetic resonance (NMR) spin-spin relaxation time (T2) relaxometry. *Canadian Geotechnical Journal, 55*(2), pp. 208-216.

[19] Kuang, K. (2018). Wireless chemiluminescence-based sensor for soil deformation detection. *Sensors and Acruators, 269*, pp. 70-78. doi:10.1016/j.sna.2017.11.017

[20] Li, Z., Escoffier, S., & Kotronis , P. (2013). Using centrifuge tests data to identify the dynamic soil properties: Application to Fontainebleau sand. *Soil Dynamics and Earthquake Engineering, 52*, pp. 77-87. doi:10.1016/j.soildyn.2013.05.004

[21] Massarsch, K. R. (2004). Deformation properties of fine-grained soils from seismic tests. Keynote lecture. *International Conference on Site Characterization, ISC'2*. Porto.

[22] Mayne, P. W., Coop, M. R., Springman, S. M., Huang, A., & Zornber, J. G. (2009). Geomaterial behaviour and testing. *Proc. of the 17-th International Conference on Soil Mechanics and Geotechnical Engineering*. Alexandia.

[23] Srokosz, P. E., Bujko, M., Bocheńska, M., & Ossowski, R. (2021). Optical flow method for measuring deformation of soil specimen subjected to torsional shearing. *Measurement, 174*, p. 109064. doi:10.1016/j.measurement.2021.109064

[24] Srokosz, P. E., Dyka, I., Bujko, M., & Bocheńska, M. (2021). A Modified Resonant Column Device for In-Depth Analysis of Vibration in Cohesive and Cohesionless Soils. *Energies, 14*(20), p. 6647. doi:10.3390/en14206647

[25] Tyrologou, P., Dudeney, A. W. & Grattoni, C. A. (2005). Evolution of porosity in geotechnical composites. *Magnetic Resonance Imaging, 23*(6), p. 765-768.

[26] White, D. J., Take, W. A., & Bolton, M. D. (2003). Soil deformation measurement using particle image velocimetry (PIV) and photogrammetry. *Geotechnique, 53*(7), pp. 619–631.

[27] Wichtmann, T. (2016). *Soil Behaviour under Cyclic Loading—Experimental Observations, Constitutive Description and Applications. [Habilitation, Karlsruhe Institute of Technology]*. Karlsruhe, Germany.

[28] Wichtmann, T., & Triantafyllidis, T. (2020). Influence of the Grain-Size Distribution Curve of Quartz Sand on the Small Strain Shear Modulus Gmax. *Journal of geotechnical and geoenvironmental engineering, 135*(10), pp. 1404-1418. doi:10.1061/(ASCE)GT.1943- 5606.0000096

[29] Xu, D. -S. (2017). A New Measurement Approach for Small Deformations of Soil Specimens Using Fiber Bragg Grating Sensors. *Sensors, 17*(5), p. 1016. doi:10.3390/s17051016